

Spatially resolved study of quantum efficiency droop in InGaN light-emitting diodes

Yue Lin,^{1,2} Yong Zhang,^{1,a)} Zhiqiang Liu,³ Liqin Su,¹ Jihong Zhang,² Tongbo Wei,³ and Zhong Chen²

¹Electrical and Computer Engineering Department, University of North Carolina at Charlotte, Charlotte, North Carolina 28223, USA

²Department of Electronic Science and Fujian Engineering Research Center for Solid-State Lighting, Xiamen University, Xiamen, Fujian 361005, People's Republic of China

³R&D Center for Semiconductor Lighting, Chinese Academy of Sciences, Beijing 100083, People's Republic of China

(Received 14 November 2012; accepted 3 December 2012; published online 17 December 2012)

We investigate the spatial variation of the external quantum efficiency (EQE) of InGaN light-emitting diodes. Two different types of EQE droop are examined in one single device, offering unambiguous analyses on the underlying material physics without the complications of the processing variation. The interplays of microscopic defects, extended defects, and energy fluctuation dictate the mechanisms of the droop, which represents a common theme in various optoelectronic devices. The two droop types correspond to the two extreme situations of energy fluctuation that affects the carrier diffusion and recombination. The finding suggests ways for improving the device performance, depending on operation conditions. © 2012 American Institute of Physics. [<http://dx.doi.org/10.1063/1.4772549>]

Typical light-emitting diodes (LEDs) based on InGaN quantum wells face the so-called “current droop” in electroluminescence (EL),^{1,2} namely, with increasing the forward driving current I_f , the external quantum efficiency (EQE) initially increases then decreases after reaching a peak at I_{max} . A number of intrinsic and extrinsic mechanisms have been proposed to explain the droop effect, including (1) Auger recombination^{3–9}; (2) carrier leakage that itself may be due to various possibilities: difference in mobility between electrons and holes, polarization field, and insufficient electron blocking between the active region and p-GaN layer at high injection level^{10–16}; (3) density activated defect recombination (DADR)¹⁷; and (4) carrier delocalization (CDL).¹⁸ DADR and CDL share the same general idea: at low current level, the carriers populate the lower energy regions, due to either In composition or well width fluctuation, where the radiative recombination dominates; whereas at high current level, the carriers start to populate the high energy regions where nonradiative loss is more prominent. Similar situations have in fact been observed in various other systems, such as GaAs quantum dots induced by lateral strain field in a GaAs/AlGaAs QW structure showing enhanced PL efficiency from the quantum dot.¹⁹ Note that the enhancement is not necessarily because the low energy region has a low defect density but primarily due to one or both of these effects: the suppressed spatial mobility reduces the probability of the carriers being captured by nonradiative centers in a larger volume and carriers from the surrounding area diffuse into the local energy minimum (LEM).

Two distinctly different types of droop behaviors are readily seen in the literature,^{18,20,21} resembling those depicted in Figure 1 of our own results. For type I, the EQE curve tends to have a slow rise or large I_{max} and decays slowly in a nearly

constant rate; for type II, the EQE exhibits a fast rise or small I_{max} , followed by an initial rapid decay, then approaching the lower decay rate similar to that of type I. The perception in the literature seems to be that type I is preferred over type II, because the decay is less between the peak and the high current value. Particularly, when two devices happen to have comparable peak EQEs, this perception is enforced,⁵ because the preference of type I is only justified if one assumes that the achievable peak EQE values are similar for the two types. Many droop curves reported in the literature resemble either type I or II, but often without giving the absolute values. Even for those cases where the absolute efficiencies were given, because of a large number of variables in device fabrication and characterization, it is not always trivial to compare two

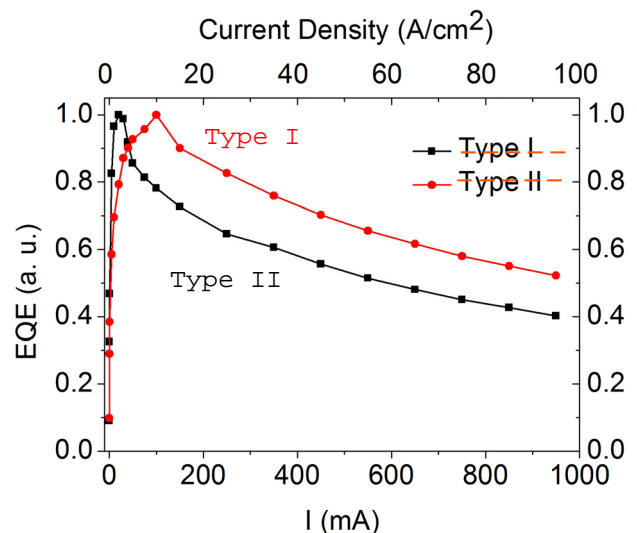


FIG. 1. Two distinctly different types of droop behaviors observed in InGaN QW LEDs. Two curves shown here are normalized results of Fig. 4(b).

^{a)}yong.zhang@uncc.edu.

independently fabricated devices. Therefore, it would be highly desirable to compare the two different droop behaviors within one single device, which is the primary goal of this work. We note that there is very little explicit discussion on the underlying mechanism and implication of the apparent larger I_{max} for the type I behavior. Our analysis indicates that seeking a large I_{max} could in fact be off on the wrong track. We point out that a high performance device should have a rapid rise of EQE to a high initial value with increasing I_f , implying a small I_{max} , and a small droop rate $\tau_{EQE} = d(EQE)/dI_f$ thereafter.

Spatially resolved optical spectroscopy methods are often used for investigating the mechanism of carrier localization to the LEMs, for instance, recent efforts using spatially resolved photoluminescence (PL) and EL^{22,23} in InGaN QW green LEDs. We have performed spatially resolved EL and PL studies on InGaN QW blue LEDs, focusing on the consequence of the energy localization on the droop instead of the specific mechanism of the localization. One device is identified to be uniquely suitable for our purpose to investigate the two distinctly different droop behaviors within one single device. This sample exhibits two types of spatially separated macroscopic regions, presumably due to unintended growth non-uniformity, which show, respectively, the two characteristic droop behaviors that are often found in two independently made devices. Interestingly but not surprisingly, a high efficiency region typically shows a low I_{max} , whereas a low efficiency region can nevertheless have significantly higher I_{max} , which is in stark contrast to the perception.

The device was grown on a free-standing GaN substrate, includes 2 μm undoped GaN, 2 μm n-GaN, buffer layer with 3 InGaN/GaN QWs (1 nm/30 nm), 5 QWs with doped barriers (3 nm/8 nm), 6 active QWs (3 nm/8 nm), 40 nm AlGaIn, and 150 nm p-GaN. The area of the active region is 1 mm^2 . The details of device fabrication can be found elsewhere.²⁴ The device has no encapsulation, because of using a short working distance microscope lens. The EQE of the bright region of this device would be comparable to those studied by some of us ($\sim 45\%$),⁵ if it were encapsulated in the same way. The defect density is $\sim 10^7 \text{ cm}^{-2}$. As typical in the literature, the defect densities quoted here are for the *extended defects* (EDs, typically threading dislocations). The concentrations of the *microscopic or point defects* (PDs)), which could be as important if not more for the device performance, are unfortunately not known, as usual.

The μ -EL measurement was performed using a Horiba LabRAM HR confocal optical system, with a 40 \times UV objec-

tive lens with NA = 0.5 or a diffraction limit spatial resolution $\sim 550 \text{ nm}$ at emission wavelength 450 nm. EL driving current, provided by a Keithley 2401 source unit, varied from 0.1 to 950 mA or 0.01 to 95 A/cm^2 , corresponding to an average carrier density of 3.5×10^{13} – $3.3 \times 10^{17} \text{ cm}^{-3}$ in the active region. A 325-nm UV laser was used as the excitation source for PL with an approximate density of $10^6 \text{ W}/\text{cm}^2$.

Figure 2 shows the EL images taken by a digital camera under different forward currents: 0.5, 3, and 100 mA, respectively. At low current, only isolated spots and regions emit weakly. With increasing current, the emitting regions expand and some gradually merge into each other. However, some areas remain relatively dark or emit only weakly even under high currents. This device appears to be highly non-uniform but in a unique way. Note that the bright and dark regions are often in macroscopic sizes (as large as tens of microns) that far exceeds the typical carrier diffusion length in this type of material. Therefore, they may be viewed as nearly independent, except for sharing the same electrodes.

Figure 3 shows the results of EL mapping under 5 mA ($< I_{max}$) in an area of $16 \mu\text{m} \times 20 \mu\text{m}$: the intensity (Fig. 3(a)) and peak energy (Fig. 3(b)) distributions, the typical EL spectra of bright and dark regions (Fig. 3(c)), and the corresponding PL spectra ($\sim 10^6 \text{ W}/\text{cm}^2$) from the same spots (Fig. 3(d)). The intensity variation between the dark and bright regions is rather high, 80%–90%. However, although there is a general anti-correlation between the emission intensity and peak energy, the variation in peak energy is relatively small, $\sim 10 \text{ meV}$. Occasionally, the dark region could have slightly higher peak energy, but within a few meV. One can assert that the average In composition and well width are more or less the same throughout the whole InGaIn layer, and thus assume homogeneous injection for both electrons and holes from n-GaN and p-GaN, respectively, to the bright and dark regions. However, on the microscopic scale, the energy fluctuation could be very different between the bright and dark regions. Specifically, the bright region seems to have more energy traps, manifesting as a low energy shoulder below the main emission peak at very low current ($< 5 \text{ mA}$) and in the PL spectrum (Fig. 3(d)). The existence of these traps and the accompanying lateral energy barriers is essential for the substantially more efficient radiative recombination from the bright region. In the dark region, the material is likely more uniform.

Two EQE curves for the whole device are given in Fig. 4(a): one measured in the convention way, and the other under a constant junction temperature of 35 $^\circ\text{C}$ using

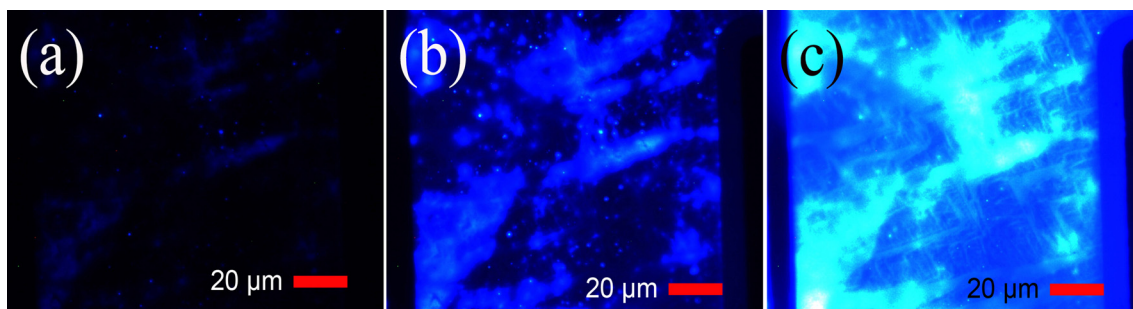


FIG. 2. The photo images of the LED operated under different forward currents: (a) 0.5 mA, (b) 3 mA, and (c) 100 mA.

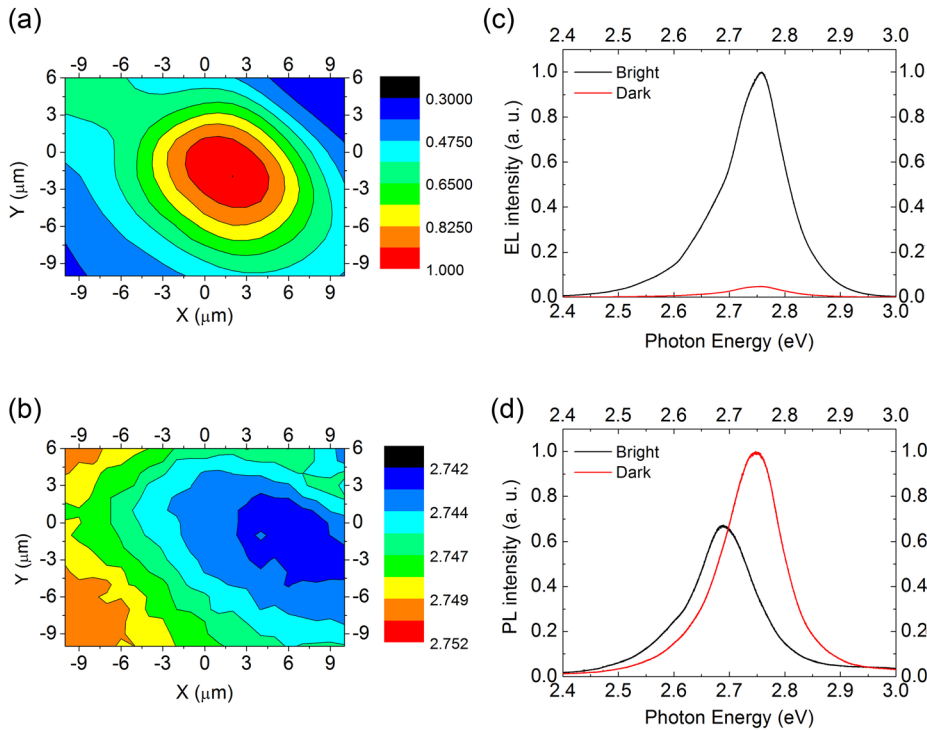


FIG. 3. EL mapping results of the LED at 5 mA: (a) EL intensity; (b) EL peak-energy; EL and PL spectra measured from the same bright and dark spots in EL: (c) EL and (d) PL.

a technique reported recently.²⁵ The ratio of the two curves is defined as “heating effect.” It is apparent that junction heating does contribute to the droop, although not the primary factor. Fig. 4(b) depicts the normalized local EQE curves with one typical bright and dark spot, measured under nominally same conditions. With the homogenous injection assumption mentioned above, the relative local EQE can be defined as the ratio of the local emission intensity and the injection current apart from a common constant. It is clear that the curves for the bright and dark regions are drastically different: the bright region resembles

the type II behavior, and the dark region resembles the type I behavior.

In the literature, the EQE- I_f curve is often described by an ABC model that includes nonradiative (A), radiative (B), and Auger (C) recombination¹² In this model, EQE is not an explicit function of I_f but through the dependence of the carrier density on I_f , and the roles of PDs and EDs are not distinguished. Here, we provide an alternative model that directly relates the EQE to I_f . We only use it to discuss the rise portion of the EQE- I_f curve, to emphasize the significance of the rise part in the whole process of droop. This is a

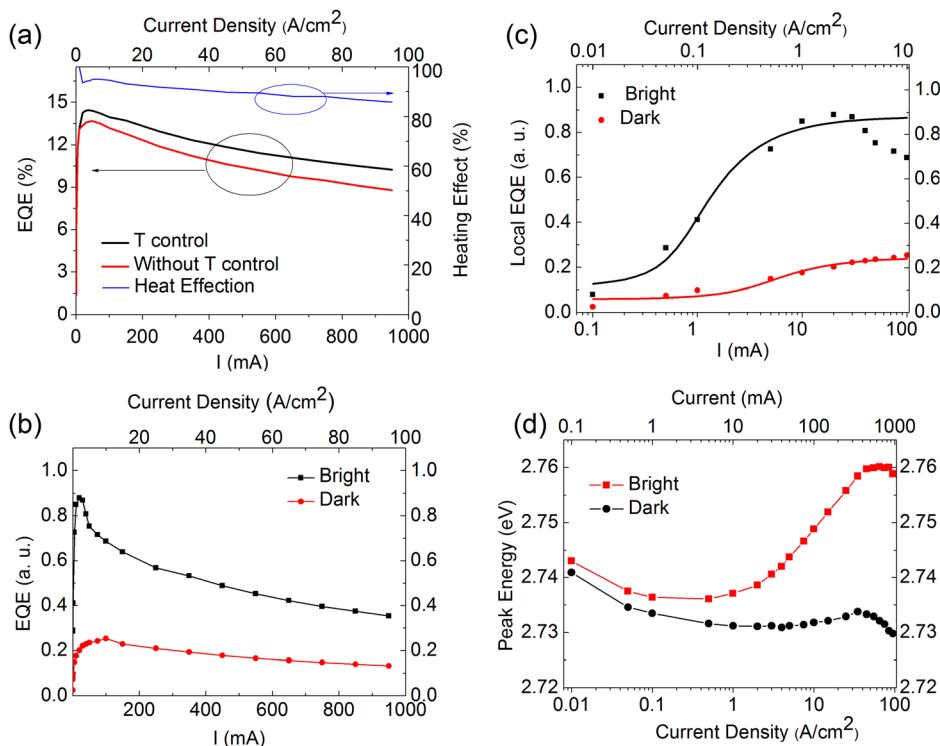


FIG. 4. (a) The whole device EQE droop curve with and without junction temperature control. The junction temperature was set to 35 °C for the controlled case. The right axis shows the ratio of the two curves—heating effect. (b) Local EQE vs. current at representative locations. (c) Fitting results for the rise part of the EQE curves. (d) The EL peak-energy shifts for the bright and dark regions.

two-level model with one representing the band edge states that contribute to the band edge emission, and the other mimicking the PD states relatively far away from the band edge states and they may recombine either radiatively or nonradiatively. We can write two rate equations¹⁹ as

$$\begin{cases} \frac{dn}{dt} = G - nW_r - n\gamma_t N_t(1-f) \\ \frac{dN}{dt} = n\gamma_t N_t(1-f) - fN_t W_t \end{cases}, \quad (1)$$

where n and N are the electron densities, respectively, for the band edge and deep defect level, N_t is the defect density, G the generation or injection rate which is proportional to I_f , W_r the radiative recombination rate, γ_t the defect capture coefficient with $c_t = \gamma_t N_t$ the capture rate, $f = N/N_t$ the defect occupation fraction, W_t the defect recombination rate. The steady state solutions of Eq. (1) yield the following equation for the internal efficiency:

$$\eta = \frac{nW_r}{G} = \frac{1}{2} \left(1 - \frac{\alpha + \beta}{G} + \sqrt{\frac{4\alpha}{G} + \left(1 - \frac{\alpha + \beta}{G}\right)^2} \right), \quad (2)$$

where $\alpha = W_r W_t / \gamma_t$ and $\beta = N_t W_t$. β represents the maximum recombination rate of the defect level, and α is an effective recombination rate of the defect level. If $N_t = 0$ or $\alpha \gg \beta$ (i.e., $W_r \gg c_t$), $\eta \rightarrow 1$. To fit the relative experimental EQE, we rewrite Eq. (2) as

$$\eta_{EQE} = \frac{nW_r}{\zeta I_f} = C \left(1 - \frac{\alpha' + \beta'}{I_f} + \sqrt{\frac{4\alpha'}{I_f} + \left(1 - \frac{\alpha' + \beta'}{I_f}\right)^2} \right), \quad (3)$$

where G is replaced by ζI_f , α and β by $\alpha' = \alpha/\zeta$ and $\beta' = \beta/\zeta$, and $1/2$ by C to include the extraction efficiency. Equation (3) can then be used to fit the experimental data of the low I_f region in Fig. 4(b). The fitted curves with comparison to the original data are showed in Fig. 4(c), with the fitting parameters list in Table I. The dark region understandably has a larger β value than the bright region, because β is the maximum recombination rate of the defect level. In the dark region, it is the large β that prevents the EQE to reach a high peak value, because the defect level could not be saturated easily even when I_f approaches 100 mA or 10 A/cm². A reasonable explanation could be that in the dark region, the carriers are more mobile, thus more susceptible to the PDs, which leads to the smaller peak EQE and larger I_{max} ; whereas in the bright region, the carriers are more localized, thus more immune from the PDs, leading to the larger EQE and smaller I_{max} . This understanding is supported by the

comparison of emission peak energy vs. I_f shown in Fig. 4(d): for the bright region, a significant blue shift or band filling occurs in roughly the 20–400 mA range, corresponding to the range of the fast droop, reflecting less nonradiative recombination and a progressive delocalization process; for the dark region, lacking of efficient localization prevents any observable blue shift.

The EQE- I_f curve for a typical InGaN LED involves at least three processes: (1) the nonradiative process caused by PDs that are more important in the low current region, because they limit the carrier mobility and thus diminish the effectiveness of the EDs,²⁶ but PDs usually can be saturated under a moderately high injection level (corresponding to the A process in the literature, although it is often implicitly assumed to be related to EDs). (2) Carrier delocalization effect that typically occurs at 2–3 A/cm² level. However, delocalization itself does not quench the radiative recombination efficiency, but the loss of these delocalized carriers through other channels does. (3) EDs that capture the carriers from the band edge states before they can radiatively recombine. Mobile carriers tend to be more vulnerable to the EDs. The above analyses of the rise process reveal the pivotal role of the PDs in setting the initial rate of the efficiency rise and its peak value. One should not take a large I_{max} as an indication of better device, because it actually means that more carriers are required to saturate the PDs, which becomes apparent from the contrast between the bright and dark regions. The energy fluctuation initially seems to help in preventing the carriers from suffering the nonradiative recombination loss through both PDs and EDs. The delocalization effect is responsible for the quick droop of the efficiency after I_{max} ,¹⁸ as in the cases of the bright region. It has been shown that the effectiveness of the ED depends quite sensitively on the carrier density, because of the diffusion length varies with the carrier density.²⁶ The EDs are relatively benign at low carrier density, because in this region, the PDs limit the carrier diffusion; they are also less effective at very high carrier density, because the carrier diffusion length decreases again at high carrier density due to the carrier lifetime reduction.²⁶ For the intermediate current range, localization can suppress the effectiveness of the EDs.²⁷ We note that even at the highest current, the bright region remains significantly more efficient than the dark region (by a factor of 2.7). The difference could be roughly interpreted as the contribution of the localization sites that can still hold a significant amount of the carriers even at a rather high current; and only those carriers spilling-over the energy traps are susceptible to the EDs.

Above discussion would suggest neither type I nor type II is the ideal option. One could envision a more desirable scenario: for a material with a low PD density and a not-so-high density of EDs (10⁶ cm⁻² or lower), the EQE - I_f curve will exhibit a fast rise to a high value followed by a slow droop with a small droop rate <0.1%/(A/cm²).²⁸ The slow decay part at the high current region is presumably due to the third process mentioned above. The relatively small τ_{EQE} for the dark region could be understood as the “intrinsic” droop rate that is determined by the density of the EDs as well as the junction heating effect. Even for the curve of bright region, despite the significant early droop, in the high

TABLE I. The fitting parameters of the two-level mode.

Parameters	Bright	Dark
α' (mA ⁻¹)	0.09	0.87
β' (mA ⁻¹)	0.61	2.78
$\beta'/\alpha' = c_t/W_r$	6.86	3.20

current region, the droop rate seems to converge to the same lower value of the dark region. Although ultimate solution for the droop effect would be to reduce the both the microscopic and extended defect densities and improve the uniformity of the active layer, a practical mitigation of the droop effect for a device expected to operate only at the moderate current level could be the design of a more effective localization scheme. The general understanding derived from this work is expected to be applicable to other types of semiconductor such as InGaP and AlGaIn based LEDs.

The work at UNC-Charlotte was supported by Bissell Distinguished Professorship, MURI/ARO (DAAD19-01-1-0591), and DARPA/MTO (W911NF-11-2-0070); at Xiamen University in part by the Major Science and Technology Project between University-Industry Cooperation in Fujian Province under Grant No. 2011H6025, NSF project under Grant No. 11104230, and Key Project of Fujian Province under Grant No. 2012H0039. We thank Dr. Haruhisa Takiguchi and Dr. D. L.-S. Dang for helpful discussions and references, and Qiong Chen and Naili Yue for technical assistance.

- ¹A. Y. Kim, W. Götz, D. A. Seigerwald, J. J. Wierer, N. F. Gardner, J. Sun, S. A. Stockman, P. S. Martin, M. R. Krames, R. S. Kern, and F. M. Steranka, *Phys. Status Solidi A* **188**, 15 (2001).
- ²J. Piprek, *Phys. Status Solidi A* **207**, 2217 (2010).
- ³Y. C. Shen, G. O. Mueller, S. Watanabe, N. F. Gardner, A. Munkholm, and M. R. Krames, *Appl. Phys. Lett.* **91**, 141101 (2007).
- ⁴M. Zhang, P. Bhattacharya, J. Singh, and J. Hinckley, *Appl. Phys. Lett.* **95**, 201108 (2009).
- ⁵Z. Q. Liu, T. B. Wei, E. Q. Guo, X. Y. Yi, L. C. Wang, J. X. Wang, G. H. Wang, Y. Shi, I. Ferguson, and J. M. Li, *Appl. Phys. Lett.* **99**, 091104 (2011).
- ⁶A. Laubsch, M. Sabathil, W. Bergbauer, M. Strassburg, H. Lugauer, M. Peter, S. Lutgen, N. Linder, K. Streubel, J. Hader, J. V. Moloney, B. Pasenow, and S. W. Koch, *Phys. Status Solidi C* **6**, S913 (2009).
- ⁷N. F. Gardner, G. O. Muller, Y. C. Shen, G. Chen, S. Watanabe, W. Götz, and M. R. Krames, *Appl. Phys. Lett.* **91**, 243506 (2007).
- ⁸E. Kioupakis, P. Rinke, K. T. Delaney, and C. G. Van de Walle, *Appl. Phys. Lett.* **98**, 161107 (2011).
- ⁹K. T. Delaney, P. Rinke, and C. G. Van de Walle, *Appl. Phys. Lett.* **94**, 191109 (2009).
- ¹⁰J. I. Shim, D. P. Han, H. Kim, D. S. Shin, G. B. Lin, D. S. Meyaard, Q. F. Shan, J. Cho, E. F. Schubert, H. Shim, and C. Sone, *Appl. Phys. Lett.* **100**, 111106 (2012).
- ¹¹B. J. Ahn, T. S. Kim, Y. Q. Dong, M. T. Hong, J. H. Song, J. H. Song, H. K. Yuh, S. C. Choi, D. K. Bae, and Y. Moon, *Appl. Phys. Lett.* **100**, 031905 (2012).
- ¹²M. H. Kim, M. F. Schubert, Q. Dai, J. K. Kim, E. F. Schubert, J. Piprek, and Y. Park, *Appl. Phys. Lett.* **91**, 183507 (2007).
- ¹³I. V. Rozhansky and D. A. Zakheim, *Phys. Status Solidi A* **204**, 227 (2007).
- ¹⁴S. P. Chang, C. H. Wang, C. H. Chiu, J. C. Li, Y. S. Lu, Z. Y. Li, H. C. Yang, H. C. Kuo, T. C. Lu, and S. C. Wang, *Appl. Phys. Lett.* **97**, 251114 (2010).
- ¹⁵X. Li, X. Ni, J. Lee, M. Wu, Ü. Özgür, H. Morkoç, T. Paskova, G. Mulholland, and K. R. Evans, *Appl. Phys. Lett.* **95**, 121107 (2009).
- ¹⁶C. Huh, J. M. Lee, D. J. Kim, and S. J. Park, *J. Appl. Phys.* **92**, 2248 (2002).
- ¹⁷J. Hader, J. V. Moloney, and S. W. Koch, *Appl. Phys. Lett.* **96**, 221106 (2010).
- ¹⁸J. X. Wang, L. Wang, W. Zhao, Z. B. Hao, and Y. Luo, *Appl. Phys. Lett.* **97**, 201112 (2010).
- ¹⁹Y. Zhang, M. D. Sturge, K. Kash, B. P. Van der Gaag, A. S. Gozdz, L. T. Florez, and J. P. Harbison, *Phys. Rev. B* **51**, 13303 (1995).
- ²⁰S. H. Han, D. Y. Lee, H. W. Shim, G. C. Kim, Y. S. Kim, S. T. Kim, S. J. Lee, C. Y. Cho, and S. J. Park, *J. Phys. D: Appl. Phys.* **43**, 354004 (2010).
- ²¹J. R. Xu, M. F. Schubert, A. N. Noemaun, D. Zhu, J. K. Kim, E. F. Schubert, M. H. Kim, H. J. Chung, S. Yoon, C. Sone, and Y. Park, *Appl. Phys. Lett.* **94**, 011113 (2009).
- ²²S. De, A. Layek, A. Raja, A. Kadir, M. R. Gokhale, A. Bhattacharya, S. Dhar, and A. Chowdhury, *Adv. Funct. Mater.* **21**, 3828 (2011).
- ²³M. Meneghini, S. Vaccari, N. Trivellin, D. D. Zhu, C. Humphreys, R. Butendheich, C. Leirer, B. Hahn, G. Meneghesso, and E. Zanoni, *IEEE Trans. Electron. Dev.* **59**, 1416 (2012).
- ²⁴J. Q. Xie, X. F. Ni, Q. Fan, R. Shimada, Ü. Özgür, and H. Morkoç, *Appl. Phys. Lett.* **93**, 121107 (2008).
- ²⁵Y. Lin, Y. L. Gao, Y. J. Lu, L. H. Zhu, Y. Zhang, and Z. Chen, *Appl. Phys. Lett.* **100**, 202108 (2012).
- ²⁶T. H. Gfroerer, Y. Zhang, and M. W. Wanlass, "A Comparison of Photoluminescence Imaging and Confocal Photoluminescence Microscopy in the Study of Diffusion near Isolated Extended Defects in GaAs," in *Proceedings of the 38th IEEE Photovoltaic Specialists Conference, Austin, Texas, USA, 3-8 June 2012* (to be published).
- ²⁷S. F. Chichibu, H. Marchand, M. S. Minsky, S. Keller, P. T. Fini, J. P. Ibbetson, S. B. Fleischer, J. S. Speck, J. E. Bowers, E. Hu, U. K. Mishra, and S. P. DenBaars, *Appl. Phys. Lett.* **74**, 1460 (1999).
- ²⁸Y. Zhao, S. Tanaka, C. C. Pan, K. Fujito, D. Feezell, J. S. Speck, S. P. DenBaars, and S. Nakamura, *Appl. Phys. Express* **4**, 082104 (2011).